



# An in situ FT-IR study of photo-oxidation of alcohols over uranyl-anchored MCM-41: Possible reaction pathways

K. Vidya<sup>a</sup>, V.S. Kamble<sup>b</sup>, N.M. Gupta<sup>b</sup>, P. Selvam<sup>a,c,\*</sup>

<sup>a</sup> Solid State and Catalysis Laboratory, Department of Chemistry, Indian Institute of Technology, Bombay, Powai, Mumbai 400 076, India

<sup>b</sup> Applied Chemistry Division, Bhabha Atomic Research Center, Trombay, Mumbai 400 085, India

<sup>c</sup> National Center for Catalysis Research, Department of Chemistry, Indian Institute of Technology, Madras, Chennai 600 036, India

Received 1 October 2006; revised 7 December 2006; accepted 11 January 2007

Dedicated to Professor Akira Miyamoto on the occasion of his 60th birthday

## Abstract

Photosensitive uranyl ions anchored onto MCM-41 mesoporous molecular sieves serve as remarkable photocatalysts in the degradation of alcohols, under ambient conditions of light, temperature, and air. The rates of conversion of alcohols to carbon dioxide was found to decrease in the order methanol > ethanol > 2-propanol > 1-propanol, with the difference in reactivity attributed to the stability of the carbon-centered radicals formed during photo-oxidation. Kinetics revealed that the photo-oxidation of alcohols followed a first-order reaction. A detailed in situ FT-IR analysis was used to identify the transient species formed during the photo-oxidation of ethanol and 2-propanol over uranyl-anchored photocatalyst. Acetic acid, ethyl acetate, and acetaldehyde were the intermediates obtained over  $\text{UO}_2^{2+}$ /MCM-41 during photo-oxidation of ethanol, whereas acetate species, methyl acetate, and acetone were detected during photo-oxidation of 2-propanol. Based on the intermediate species formed, their growth with respect to irradiation time, and their intensities, appropriate reaction mechanisms were proposed to corroborate our observations.

© 2007 Published by Elsevier Inc.

**Keywords:** Mesoporous; MCM-41; Uranyl; Alcohols; Photo-oxidation; In situ IR

## 1. Introduction

Alcohols in general are known to be innocuous air pollutants. For example, methanol, which is produced naturally from biomass and fossil fuels and is widely used as solvents and fuel additives, has been identified as a serious neurotoxin that can be detrimental to human health. Other alcohols, such as ethanol, propanol, and butanol, are also considered highly toxic when inhaled [1]. The degradation of these organics is thus of paramount importance. Abatement technologies, such as incineration (thermal oxidation) and catalytic oxidation, have been used in the past for the complete oxidation of volatile organic compounds (VOCs) [2]. However, these methods require high temperatures (in the range of 300–600 °C) and often culminate in incomplete oxidation of waste stream, resulting in the forma-

tion of toxic byproducts, such as dioxins [3], dibenzofurans [4], and oxides of nitrogen [2].

In contrast to the above techniques, heterogeneous photocatalytic oxidation has drawn considerable interest from researchers, owing to its operation under mild conditions of temperature and pressure, as well as in the presence of light, and the most prevalent oxidant,  $\text{O}_2$  [5,6]. However, most of the photocatalysts used are the conventional semiconductor oxides/sulfides, which suffer from disadvantages such as absorption in the UV region and electron-hole recombination, limiting their quantum efficiency and photo-oxidation rate, thus leading to the formation of partial oxidation products [7]. In this regard, the use of photosensitive uranyl ions ( $\text{UO}_2^{2+}$ ) would seem appropriate, because their lowest excited eigenvalue ( $^*\text{UO}_2^{2+}$ ) is known to be strongly oxidizing ( $E^0 = 2.6$  V) and luminescent, and is easily quenched by various organic substrates by an electron- or atom-transfer process [8,9]. Furthermore, the visible region absorption of the uranyl ions (380–500 nm), in addition to UV

\* Corresponding author.

E-mail addresses: [selvam@iitb.ac.in](mailto:selvam@iitb.ac.in), [selvam@iitm.ac.in](mailto:selvam@iitm.ac.in) (P. Selvam).

region (200–380 nm), serves as a potential photocatalyst for air-pollution control under solar irradiation [8].

In view of the high photosensitivity of  $\text{UO}_2^{2+}$  and its absorption in the visible region of the solar spectrum, a number of studies have been carried out to study the homogeneous photo-oxidation reactions of hydrocarbons [10], chlorophenols [11], and substituted phenols [12] by uranyl ions. Comparatively, fewer studies have been devoted to the photocatalytic activity of  $\text{UO}_2^{2+}$  ions in the heterogeneous reaction mode. For instance, Suib and co-workers [13,14] used uranyl-exchanged clays and zeolites for the photo-oxidation of ethanol, isopropyl alcohol, and diethyl ether solutions to yield the corresponding aldehydes and ketones. In another study, Dai and co-workers [15] reported the photocatalytic oxidation of ethanol solution by  $\text{UO}_2^{2+}$ -doped glass, resulting in the formation of acetaldehyde. In the above cases, only partial oxidation products were obtained, due to the possible formation of photo-inactive U(IV) species during the photo-oxidation process [15].

In an attempt to effect complete oxidation of alcohols, we recently demonstrated that uranyl ions anchored onto mesoporous silicates behave as highly efficient heterogeneous photocatalysts in the vapor-phase degradation of methanol, methane, and aromatics, such as benzene, under ambient sunlight conditions [16–18]. In this study, in situ EPR and fluorescence studies showed that the  $\text{UO}_2^{2+}$  ions were replenished during the photo-oxidation process by auto-oxidation of the unstable U(V) species formed [16]. The reoxidation of U(V) to U(VI) was thus responsible for complete degradation of methanol.

In the present study, we investigated the photocatalytic behavior of  $\text{UO}_2^{2+}$  toward the oxidation of alcohols such as methanol, ethanol, 1-propanol, and 2-propanol, to demonstrate their effectiveness in the complete destruction of VOCs under irradiation. We also explored the kinetics of the photo-oxidation of alcohols and found that the reaction follows a first order in all cases. Furthermore, we carried out the first detailed in situ FTIR analysis to identify the transient species/gaseous products formed over  $\text{UO}_2^{2+}$ /MCM-41 during the photo-oxidation of ethanol and 2-propanol. We proposed appropriate photocatalytic routes, elucidating the role of  $^*\text{UO}_2^{2+}$ .

## 2. Experimental

### 2.1. Catalyst preparation

The uranyl-anchored MCM-41 catalyst was prepared by a direct template-exchange method, using a uranyl nitrate solution of 0.005 M adjusted to pH of 5.0, according to a procedure described elsewhere [19]. The uranyl-anchored MCM-41 thus obtained is designated  $\text{UO}_2^{2+}$ /MCM-41.

### 2.2. Catalyst characterization

Powder X-ray diffraction (XRD),  $\text{N}_2$ -adsorption, diffuse reflectance ultraviolet–visible (DRUV–vis), and fluorescence spectroscopy techniques were used for the characterization of bare MCM-41 and the corresponding uranyl-loaded MCM-41

Table 1  
Physical characteristics of  $\text{UO}_2^{2+}$ /MCM-41 and MCM-41

Sample	XRD		$\text{N}_2$ sorption data		
	$d_{100}$ (Å)	$a_0$ (Å)	BET surface area ( $\text{m}^2 \text{g}^{-1}$ )	Mean pore diameter (Å)	Pore volume ( $\text{ml g}^{-1}$ )
MCM-41	35.30	40.76	1032	28.2	0.90
$\text{UO}_2^{2+}$ /MCM-41	37.10	42.84	612	27.0	0.65

samples. The XRD patterns were obtained on a Rigaku diffractometer, using Ni-filtered  $\text{CuK}\alpha$  radiation, at a scan speed of  $0.5^\circ/\text{min}$  and a step size of  $0.02^\circ$ . The data on BET surface area, pore volume, and pore size distribution were obtained using a Quantachrome Autosorb-1 analyzer. About 100 mg of sample was used for this purpose. Before  $\text{N}_2$  adsorption, the sample was degassed under vacuum (10–6 Torr) at 573 K for 6 h. The DRUV–vis spectra were recorded in 200–700 nm range, using a Jasco 605 spectrophotometer. Fluorescence measurements were made on a Perkin Elmer LS-55 spectrophotometer, with an excitation radiation of 310 nm. The amount of uranium loaded in the mesoporous matrix was determined by inductively coupled plasma–atomic emission spectroscopy (ICP–AES) on a Labtam Plasma Lab 8440 and was found to be  $\sim 9.8 \text{ wt\%}$ . The physical characteristics of  $\text{UO}_2^{2+}$ /MCM-41 are listed in Table 1.

### 2.3. Catalytic activity measurements

Room temperature vapor-phase photoreaction of methanol, ethanol, 1-propanol, and 2-propanol in air (0.1–1.5 vol%) was carried out over uranyl-incorporated catalyst in static mode and in the presence of simulated light (400 W medium-pressure Hg lamp) at ambient temperatures (30–35 °C). The reaction cell (15 mm i.d., 150 mm long) was sealed at the top with the aid of a rubber septum. About 100 mg of catalyst sample was dispersed uniformly in the reaction cell and degassed appropriately before introduction of the reactants. The final pressure was kept at around 1.2 bar. A Chemito 8510 gas chromatograph, equipped with a thermal conductivity detector (set at 120 °C) and a Porapak-Q (100 °C) or Sperocarb (100 °C) column, was used for analysis of reactants and products. The average photon flux of Hg lamp, as measured by uranyl oxalate actinometry [20], was found to be  $\sim 6.5 \times 10^{14} \text{ photon s}^{-1} \text{ cm}^{-2}$ .

### 2.4. In situ FT-IR

FTIR studies were performed using a Jasco 610 spectrophotometer for in situ monitoring of the surface species and gaseous products formed over uranyl-containing mesoporous samples during the photo-oxidation reaction [21]. An ultraviolet lamp (tungsten-halogen lamp) was placed in a way so as to direct the light vertically over the catalyst wafer. An arrangement was made to pretreat the catalyst by simultaneous pumping and heating at a controlled temperature of up to  $\sim 300^\circ\text{C}$ . The cell was also equipped with a flow-through or pulse-mode introduction of a gas stream and for subsequent digital measurement of gas pressure in the range of 0 to 760 Torr. The

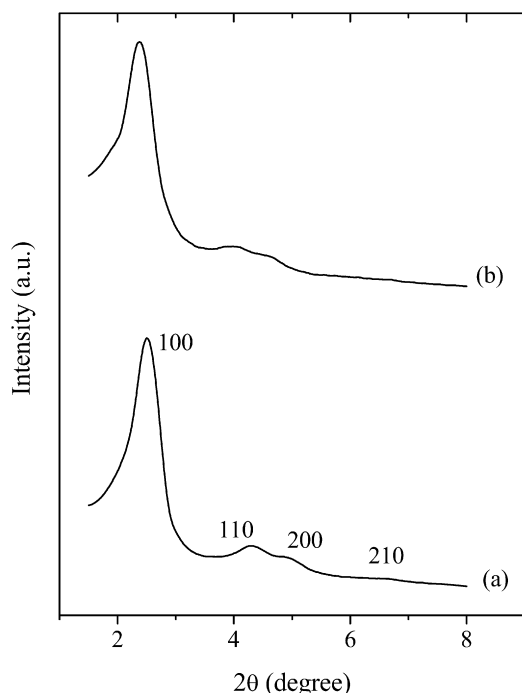


Fig. 1. Powder XRD patterns of (a) MCM-41 and (b)  $\text{UO}_2^{2+}/\text{MCM-41}$ .

4-cm-diameter  $\text{CaF}_2$  disks, placed between two pairs of water-cooled circular flanges at the two sides of the IR cell, served as windows for mid-IR region measurements. A self-supported catalyst wafer was activated under vacuum at  $\sim 200^\circ\text{C}$  before being exposed to the organics at room temperature. The organic vapors were prepared using 2 vol% in air. The spectra were collected after compensating for the IR spectrum of the unexposed pellet. The reaction was monitored after introduction of organics plus air, with respect to irradiation time.

### 3. Results and discussion

#### 3.1. Sample characteristics

Powder XRD patterns of  $\text{UO}_2^{2+}/\text{MCM-41}$  exhibited four reflections (Fig. 1b), characteristic of hexagonal MCM-41 (Fig. 1a). A decrease in intensity was observed in the XRD lines of  $\text{UO}_2^{2+}/\text{MCM-41}$  compared with parent MCM-41, due to the bridge-bonding of uranyl species with silanol groups, as well as partial structural decomposition [22]. The physical characteristics of parent MCM-41 and  $\text{UO}_2^{2+}/\text{MCM-41}$ , including surface area, pore size distribution, and pore volume, are given in Table 1. The decreases in surface area, pore volume, and pore diameter are due to uranium loading/incorporation of uranyl species in the pores of the host matrix, which causes contraction of the molecular sieve pores by bridge-bonding of uranyl species with silanol groups [23]. These decreases also could be due to the partial decomposition of the structure.

The DRUV-visible spectrum of the uranyl sample showed broad bands centered at 290 and 425 nm with shoulders at 325 and 475 nm (Fig. 2), whereas the emission spectrum exhibited broad transitions between 450 and 600 nm (not shown). The presence of these broad, overlapping absorption and emission bands instead of the well-defined, sharp transitions of parent uranyl salt (see inset in Fig. 2) in the 350–500 nm region due to electron-vibration interactions [8,9,24] is normally accepted as an evidence for binding of the uranyl species with the host matrix in the equatorial plane of  $\text{O}=\text{U}=\text{O}$ , preserving the linearity of the axial bond. The DRUV-visible results of this study thus reveal that the uranyl ions anchored in MCM-41 retain their linear symmetry, similar to that in an aqueous solution.

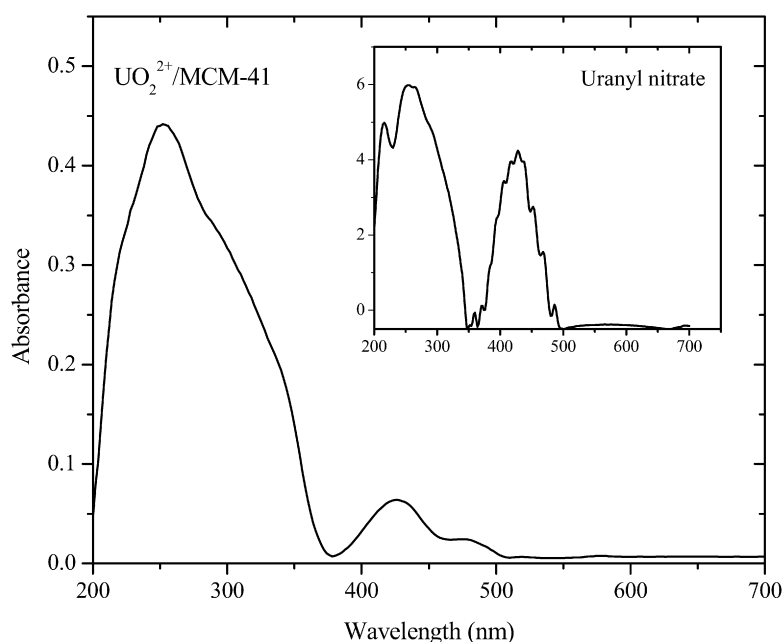


Fig. 2. DRUV-vis spectrum of  $\text{UO}_2^{2+}/\text{MCM-41}$ . Inset shows the spectrum of parent uranyl nitrate.

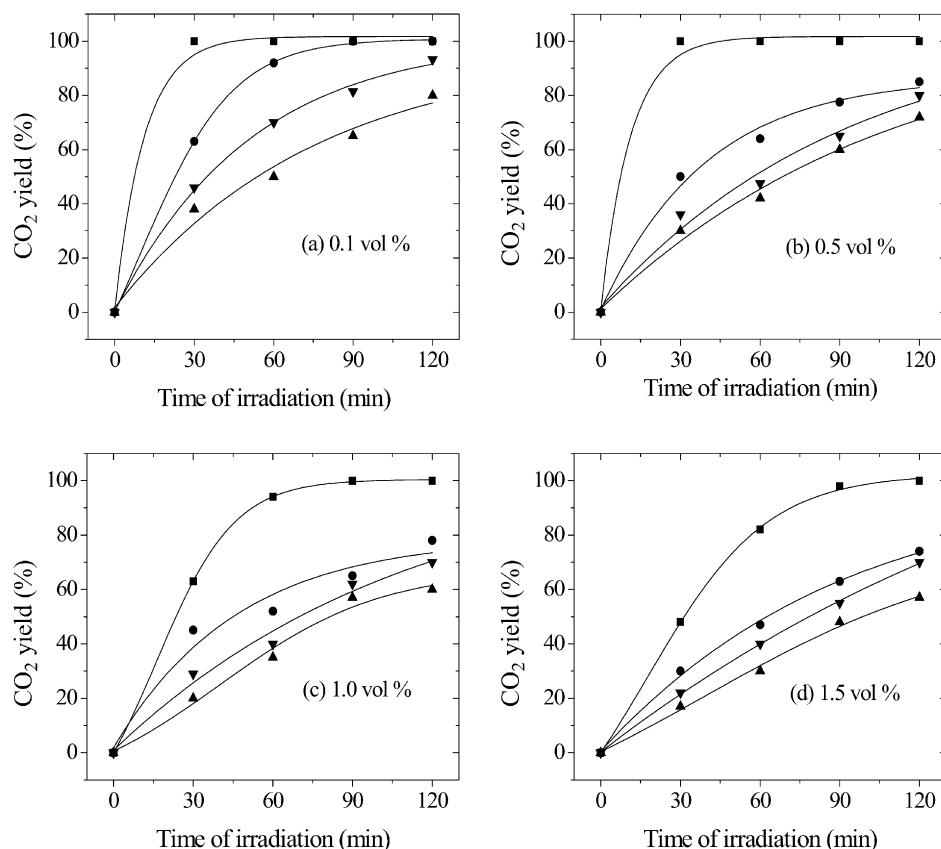


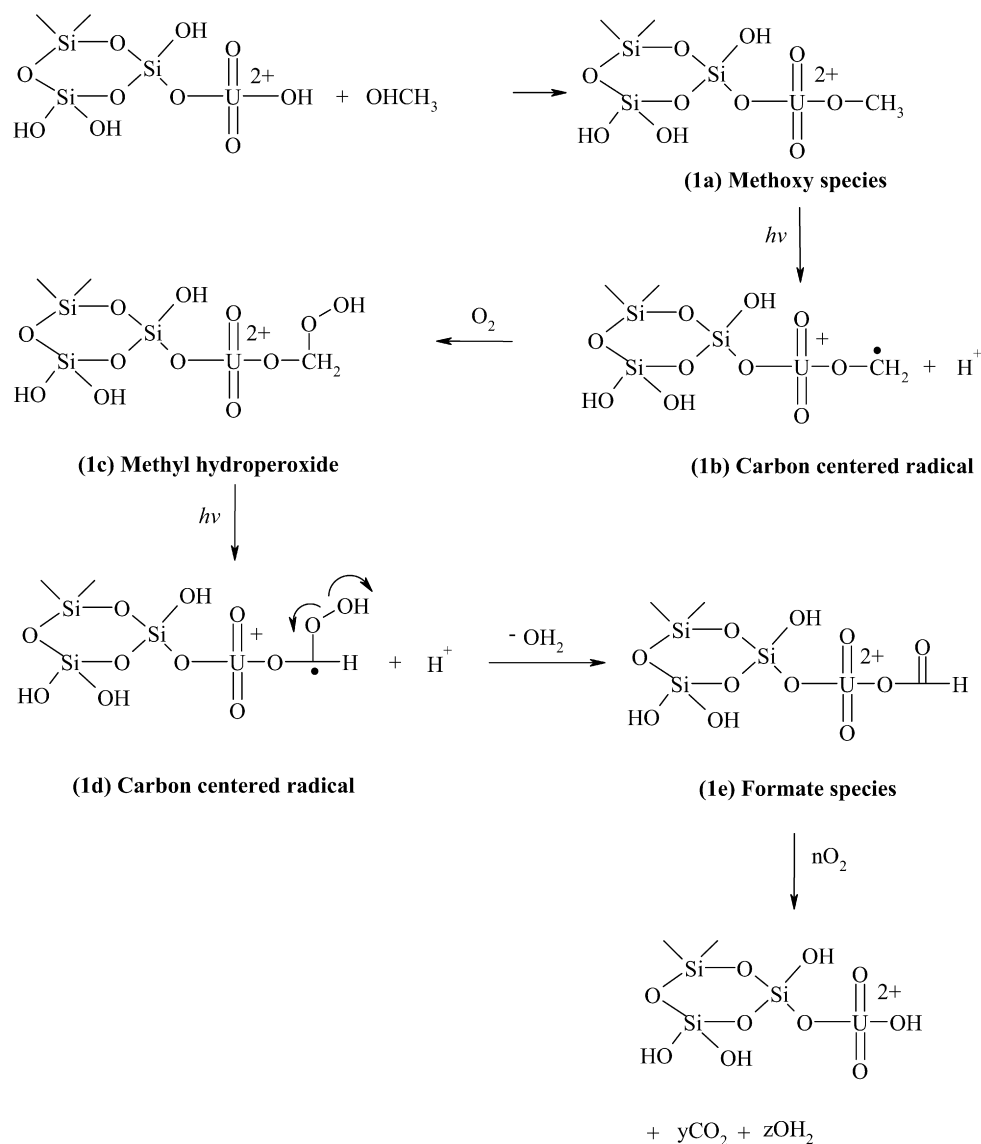
Fig. 3. Photo-oxidation of alcohols over  $\text{UO}_2^{2+}/\text{MCM-41}$  in the presence of Hg lamp (quartz cell) for varying concentrations in air (0.1–1.5 vol %): (■) methanol, (●) ethanol, (▲) 1-propanol, (▼) 2-propanol.

### 3.2. Vapor-phase photocatalytic oxidation of alcohols over $\text{UO}_2^{2+}/\text{MCM-41}$

Fig. 3 represents time-dependent variations in CO<sub>2</sub> yield obtained from the photo-oxidation of methanol, ethanol, 1-propanol, and 2-propanol over  $\text{UO}_2^{2+}/\text{MCM-41}$  for varying concentrations in air (0.1–1.5 vol %) under a medium-pressure mercury lamp and at ambient temperatures. For all the alcohols, complete degradation to carbon dioxide and water was observed, and no partially oxygenated products were detected. The extent of conversion depended on the initial concentration of alcohol vapors in air, with the reaction completed more rapidly for lower concentrations (0.1 and 0.5 vol %), as shown in Figs. 3a and 3b. It is important to note that the photo-oxidation of alcohols did not result in the formation of carbon dioxide in experiments conducted on the uranyl-free MCM-41 sample. Similarly, no reaction occurred during the room-temperature exposure of these alcohols over  $\text{UO}_2^{2+}/\text{MCM-41}$  under identical test conditions, but in the absence of irradiation. Further experiments conducted using bulk uranium oxide,  $\alpha\text{-U}_3\text{O}_8$ , also did not result in the formation of carbon dioxide. These results thus provide evidence for the crucial role of the highly dispersed  $\text{UO}_2^{2+}$  in the photocatalytic oxidation process [16–18].

The rate of conversion of alcohols to carbon dioxide was found to decrease in the order methanol > ethanol > 2-propanol > 1-propanol. We demonstrated earlier, with the help of

in situ IR experiments, that the strongly adsorbed methoxy groups on the  $\text{UO}_2^{2+}/\text{MCM-41}$  catalyst undergo H-atom abstraction by  $^*\text{UO}_2^{2+}$ , resulting in a carbon-centered radical (Scheme 1) [16]. The stability of these carbon-centered radicals thus determines the ease or difficulty with which formation of the subsequent transient species occurs, which ultimately results in complete degradation to carbon dioxide. The stability of carbon-centered radicals has been reported to follow the order methyl < 1° < 2° < 3° (see Table 2) [25]. Thus, H-atom abstraction by  $^*\text{UO}_2^{2+}$  takes place from a carbon atom, which results in the formation of the most stable radical. For example, in ethanol and 1-propanol, the H-atom abstraction forms a 1° radical, whereas in 2-propanol, it results in the formation of a 2° radical, which is more stable. Thus, according to the stability of the carbon-centered radicals formed, the rates of formation of carbon dioxide from the alcohols should follow the order methanol > ethanol > 1-propanol > 2-propanol. The discrepancy in rates of carbon dioxide formation between 1-propanol and 2-propanol in the present study could be attributed to the stability of the intermediate/transient species formed during photo-oxidation. But because in situ IR analysis was not carried out for 1-propanol, it is not possible to claim that the nature and stability of intermediate species play important roles; work along these lines is in progress. Consequently, in this study, we attribute the difference in photoactivity only to the stability of the carbon-centered radicals formed.

Scheme 1. Photo-oxidation of methanol over  $\text{UO}_2^{2+}/\text{MCM-41}$ .Table 2  
Enthalpy of formation of free radicals [25]

Free radical	$\Delta_f H^0$ (kJ mol <sup>-1</sup> )
$\text{CH}_2\text{OH}\cdot$	$-17.8 \pm 1.3$
$\text{CH}_3\text{CH}_2\text{OH}\cdot$	$-51.6 \pm 0.0$
$\text{CH}_2\text{CH}_2\text{OH}\cdot$	$-36.0 \pm 0.0$
$(\text{CH}_3)_2\text{COH}\cdot$	$-111.3 \pm 4.6$

### 3.3. Kinetics of photo-oxidation of alcohols over $\text{UO}_2^{2+}/\text{MCM-41}$

Fig. 4 plots the rate of reaction (initial rates) versus the initial concentration of alcohols. From these linear plots, it can be inferred that the photo-oxidation of alcohols follows a first-order reaction. Fig. 5 presents a logarithmic plot of rate of reaction versus initial concentration of alcohols; Table 3 gives the rate constants derived from these data. The rate constants decrease in the same order as the photocatalytic conver-

sion to carbon dioxide: methanol > ethanol > 2-propanol > 1-propanol.

### 3.4. In situ FT-IR study of photo-oxidation of alcohols over $\text{UO}_2^{2+}/\text{MCM-41}$

In this section we discuss the transient species formed over  $\text{UO}_2^{2+}/\text{MCM-41}$  during the photo-oxidation of alcohols by in situ FTIR spectroscopy analyses.

#### 3.4.1. Ethanol

Fig. 6 shows the in situ FT-IR spectra of the photo-oxidation of ethanol adsorbed over  $\text{UO}_2^{2+}/\text{MCM-41}$  before and after irradiation in the stretching and deformation regions. The samples were recorded in dry air and at room temperature. In Fig. 6, the reference/background was taken as  $\text{UO}_2^{2+}/\text{MCM-41}$  + dry air, and thus the positive bands observed in the spectra corresponded to those due to ethanol and other surface complexes formed during photo-oxidation. Meanwhile, negative bands in-

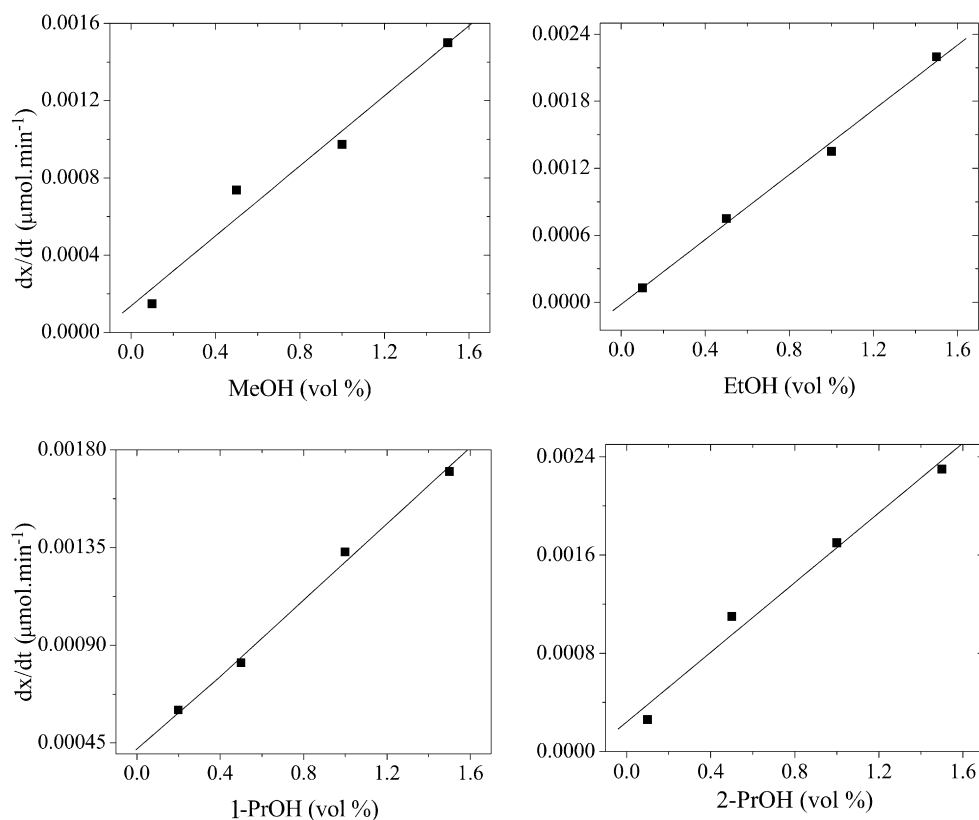


Fig. 4. Plot of rate of reaction versus initial concentration of alcohol.

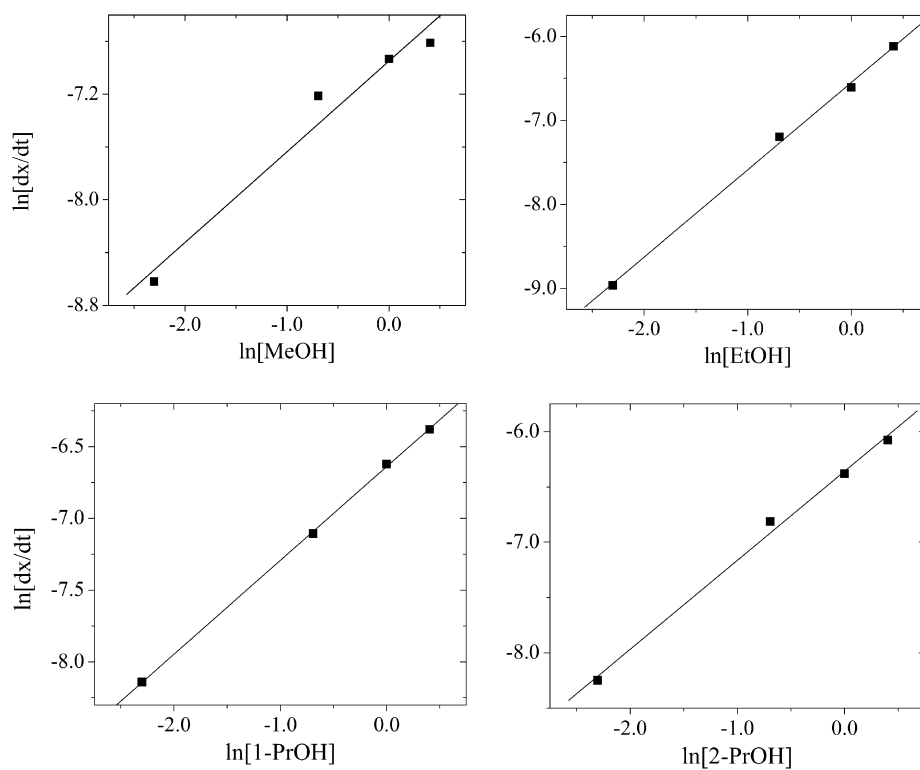


Fig. 5. Logarithmic plot of rate of reaction versus concentration of alcohol.

dicating depletion of adsorbed species. Fig. 7 shows the results of spectra of  $\text{UO}_2^{2+}/\text{MCM-41}$  + ethanol in the absence of irradiation.

Here the bands shown are due solely to the surface com-



Table 3  
Rate constants of photo-oxidation of alcohols over  $\text{UO}_2^{2+}/\text{MCM-41}$

Alcohol	$k$ ( $\text{min}^{-1}$ )
Methanol	$0.97 \times 10^{-4}$
Ethanol	$0.71 \times 10^{-4}$
2-Propanol	$0.58 \times 10^{-4}$
1-Propanol	$0.43 \times 10^{-4}$

plexes/gaseous products generated during the photo-oxidation process.

In the absence of irradiation, the adsorption of ethanol over  $\text{UO}_2^{2+}/\text{MCM-41}$  reached equilibrium in 15 min, as shown in Fig. 6. Positive bands can be seen at  $\sim 2977$ ,  $\sim 2934$ ,  $\sim 2901$ ,  $\sim 1474$ ,  $\sim 1448$ ,  $\sim 1389$ , and  $\sim 1325 \text{ cm}^{-1}$ , corresponding to the stretching and bending vibrations of molecularly adsorbed ethanol and/or ethoxide species, as outlined in Table 4 [26–31]. Further, the presence of a band at  $\sim 1250 \text{ cm}^{-1}$ , corresponding to the O–H bending vibration of adsorbed ethanol [28] indicates that part of the ethanol is molecularly adsorbed on the catalyst as  $\text{U-OH} \cdots \text{OH-CH}_2\text{-CH}_3$ , and part of it forms an ethoxide on uranyl group as  $\text{U-O-CH}_2\text{-CH}_3$  [26]. That the ethoxide species are involved in bonding with  $\text{UO}_2^{2+}/\text{MCM-41}$  is confirmed by the fact that the negative M–OH band ( $\text{U-OH/Si-OH}$ ) seen at  $\sim 3734$  and  $\sim 3673 \text{ cm}^{-1}$  is due to depletion of isolated hydroxyl groups (Fig. 7) [26]. However, the band assignments of Si–OH and U–OH remain ambiguous. Further, a broad band was observed at  $\sim 3171 \text{ cm}^{-1}$  due to the  $\nu(\text{OH})$  vibration of hydrogen-bonded ethanol to the photocatalyst [16,26,29], confirming the presence of molecularly adsorbed ethanol. In addition, a band at  $\sim 1627 \text{ cm}^{-1}$ , due to  $\delta(\text{OH})$  of adsorbed water [29–31], indicates the formation of ethoxide with  $\text{UO}_2^{2+}/\text{MCM-41}$ . Exposure of ethanol to the photocatalyst in the absence of irradiation did not result in the formation of any new bands (Fig. 6) [16].

Under irradiation, the FTIR spectrum of  $\text{UO}_2^{2+}/\text{MCM-41}$  + ethanol exhibited a number of changes, as shown in Figs. 6 and 7. The highlights of these results are as follows:

- (i) Various new IR bands began to develop on irradiation and increased in intensity with time, as shown in Figs. 6 and 7; these bands and their assignments are listed in Table 5. A band at  $\sim 1759 \text{ cm}^{-1}$  was observed, in addition to a sharp peak at  $\sim 1744 \text{ cm}^{-1}$  and a shoulder at  $\sim 1726 \text{ cm}^{-1}$ . Based on data in the literature, the band at  $\sim 1759 \text{ cm}^{-1}$  is assigned to the  $\nu(\text{C=O})$  of acetic acid [29–31], and those observed at  $\sim 1744$  and  $\sim 1726 \text{ cm}^{-1}$  are due to the  $\nu(\text{C=O})$  of methyl acetate [29–31] and acetaldehyde [26, 27,29–31], respectively. Further, a broad band was seen at  $1480\text{--}1420 \text{ cm}^{-1}$ , which could be due to overlapping IR bands of  $\delta(\text{OH})$  of acetic acid ( $\sim 1442 \text{ cm}^{-1}$ ) [29–31] and  $\delta_{\text{as}}(\text{CH}_3)$  of acetaldehyde ( $\sim 1428 \text{ cm}^{-1}$ ) [27,29–31]. In addition, a band at  $\sim 1387 \text{ cm}^{-1}$  could be assigned to the  $\delta(\text{CH}_2)$  of ethyl acetate, and a band at  $1348 \text{ cm}^{-1}$  was due to  $\delta_{\text{as}}(\text{CH}_3)$  of acetaldehyde [27,29–31]. The presence of acetaldehyde is further validated by the  $\nu(\text{C-H})$  at  $\sim 2927$  and  $\sim 2693 \text{ cm}^{-1}$  [29]. The formation of acetic

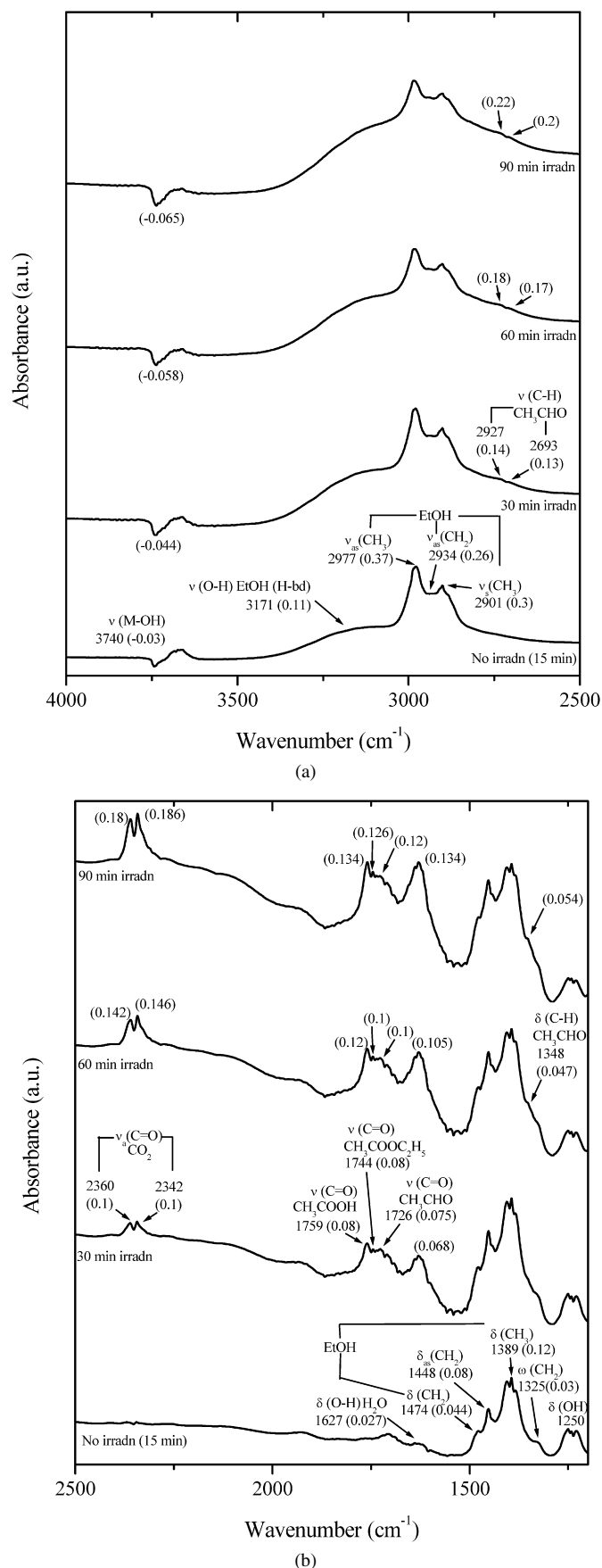


Fig. 6. FT-IR spectra of  $\text{UO}_2^{2+}/\text{MCM-41}$  with ethanol prior to and post irradiation in the (a) stretching and (b) deformation regions.

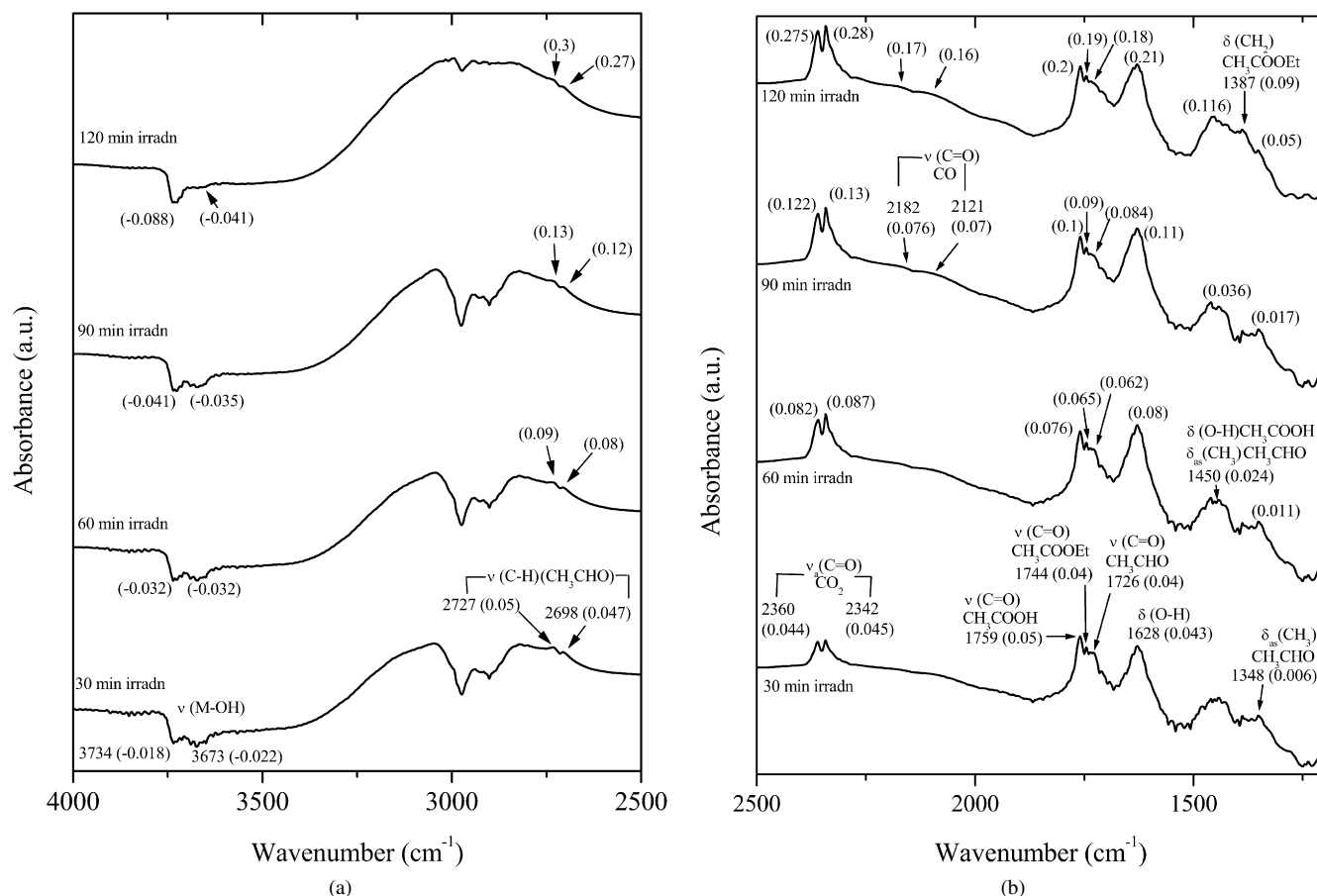


Fig. 7. Subtracted spectra of  $\text{UO}_2^{2+}/\text{MCM-41} + \text{ethanol}$ , under irradiation in the (a) stretching and (b) deformation region. The spectra of  $\text{UO}_2^{2+}/\text{MCM-41} + \text{ethanol}$  in the absence of irradiation is taken as the reference/background.

Table 4  
Assignment of the FT-IR bands of ethanol/ethoxide adsorbed on  $\text{UO}_2^{2+}/\text{MCM-41}$  in dry air at room temperature in the absence of irradiation

Frequency (cm <sup>-1</sup> )			Vibrational mode
This work	Reported [26–28]		
	Ethanol	Ethoxide	
3171	3550–3200	–	$\nu(\text{OH})$ , H-bonded
2977	2971, 2980	–	$\nu_{\text{as}}(\text{CH}_3)$
2934	2931	–	$\nu_{\text{as}}(\text{CH}_2)$
2901	2868, 2897	–	$\nu_{\text{s}}(\text{CH}_3)$
1474	1474	1474	$\delta(\text{CH}_2)$
1448	1447, 1453	1447, 1451	$\delta_{\text{as}}(\text{CH}_3)$
1389	1379, 1381	1379, 1380	$\delta_{\text{s}}(\text{CH}_3)$
1325	1333, 1356	1356	–CH <sub>2</sub> – wag
1250	1274, 1264 [28]	–	$\delta(\text{OH})$

acid over  $\text{UO}_2^{2+}/\text{MCM-41}$  is a possible indication of the fact that photoreaction occurs over adsorbed ethanol (hydrogen bonded) rather than on ethoxide, as demonstrated by the broad bands at  $\sim 3171 \text{ cm}^{-1}$  (H-bonded OH of ethanol) and  $\sim 1250 \text{ cm}^{-1}$  ( $\delta_{\text{OH}}$  of ethanol).

- (ii) IR bands due to carbon dioxide, carbon monoxide, and water were also formed during the photo-oxidation of ethanol and increase in intensity with irradiation time, congruent with our photocatalytic results. The presence of two  $\nu_{\text{a}}(\text{C}=\text{O})$  bands for carbon dioxide at  $\sim 2360$  and

Table 5  
Assignment of FT-IR bands generated during the photocatalytic oxidation of ethanol over  $\text{UO}_2^{2+}/\text{MCM-41}$

Frequency (cm <sup>-1</sup> )		Vibrational mode	Transient species/ gaseous products
This work	Reported		
1759	1760 [29]	$\nu(\text{C}=\text{O})$	Acetic acid
1480–1420	1440–1395 [29]	$\delta(\text{O}-\text{H})$	
1744	1750–1735 [29]	$\nu(\text{C}=\text{O})$	Ethyl acetate
1387	1400–1340 [29]	$\delta(\text{CH}_2)$	
2727, 2698	2830–2695 [29]	$\nu(\text{C}-\text{H})$	Acetaldehyde
1726	1730 [29], 1715 [26,27]	$\nu(\text{C}=\text{O})$	
1480–1420	1428 [27]	$\delta_{\text{as}}(\text{CH}_3)$	
1348	1351 [27]	$\delta_{\text{s}}(\text{CH}_3)$	
2360, 2342	2349 [30,31]	$\nu_{\text{as}}(\text{C}=\text{O})$	Carbon dioxide
2182, 2121	2127 [30,31]	$\nu(\text{C}=\text{O})$	Carbon monoxide
1627	1630 [30,31]	$\delta(\text{O}-\text{H})$	Water

$\sim 2342 \text{ cm}^{-1}$  (literature value,  $2349 \text{ cm}^{-1}$ ) [29–31] indicates that  $\text{CO}_2$  is present in both gaseous and bonded forms (Table 5). The same argument also holds for the two bands observed for carbon monoxide at  $\sim 2182$  and  $\sim 2121 \text{ cm}^{-1}$  (literature value,  $2127 \text{ cm}^{-1}$ ).

- (iii) The growth of IR bands due to acetaldehyde, acetic acid, and ethyl acetate was plotted as a function of irradiation time and is presented in Fig. 8a. It can be seen that these



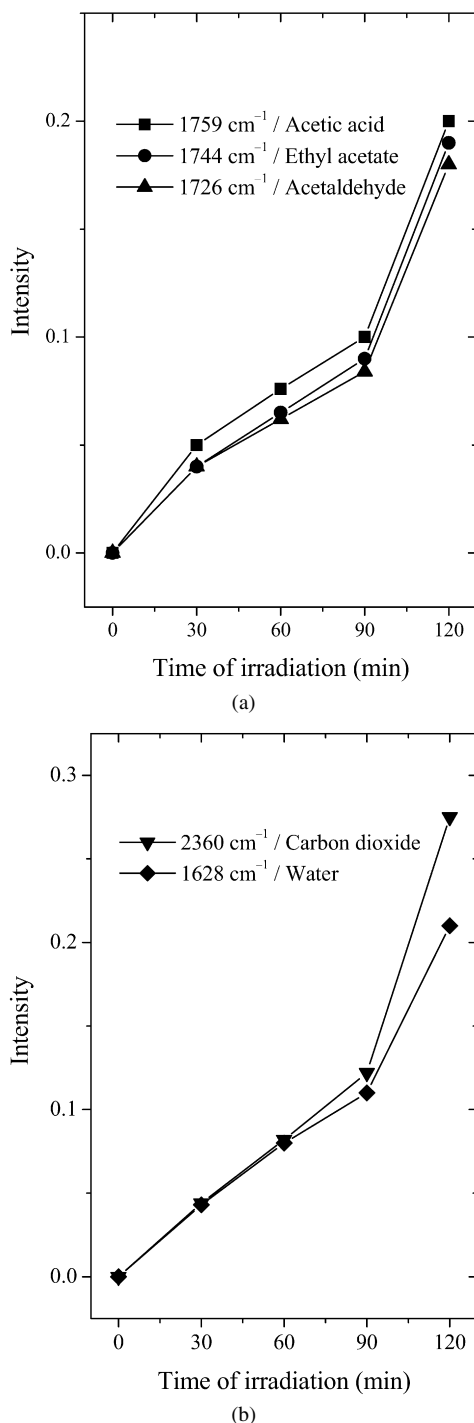


Fig. 8. Plot of intensities of (a) transient species and (b) gaseous products formed during photo-oxidation of ethanol over  $\text{UO}_2^{2+}/\text{MCM-41}$ , as a function of irradiation time.

bands increased in intensity with time, with a sharp rise after 90 min of irradiation, indicating increased photo-oxidation of ethanol to the intermediate species acetaldehyde, acetic acid, and ethyl acetate. This could be due to the greater availability of photoactive sites. The intensities of acetic acid, ethyl acetate, and acetaldehyde were found to be nearly equal and to follow a similar time profile, indicating that their production from ethanol occurs

in independent reaction pathways. The next section discusses the reaction mechanisms in detail. Fig. 8b shows the growth of IR bands due to carbon dioxide and water, conforming to our photocatalytic results.

- (iv) From Fig. 7, it can be seen that the  $\nu(\text{M-OH})$  band at  $\sim 3734 \text{ cm}^{-1}$  becomes more negative in intensity on irradiation with time compared with the band at  $3673 \text{ cm}^{-1}$ . The near-constant absorbance value of the band at  $3673 \text{ cm}^{-1}$  leads us to believe that it is due to the non-participation of the silanol groups ( $\text{Si-OH}$  and  $\text{Si-OEt}$ ) during the photocatalytic oxidation process in comparison with  $\text{UO}_2^{2+}$ , thus establishing the importance of the reaction occurring only at the uranyl site. During photo-oxidation of ethanol/ethoxide on the  $\text{UO}_2^{2+}$  site, the formation of transient species (e.g., ethyl acetate, acetaldehyde) possibly leads to a stronger bond formation with the uranyl catalyst compared with ethanol, thus resulting in higher negative values, as indicated in Fig. 7.
- (v) Identical experiments conducted over a parent MCM-41 sample did not result in the formation of additional bands (not shown here), highlighting the importance of  $\text{UO}_2^{2+}$  ions in a photocatalytic process [16].

### 3.4.2. 2-Propanol

Fig. 9 shows the in situ IR spectra of  $\text{UO}_2^{2+}/\text{MCM-41} + 2$ -propanol before and after irradiation in the stretching and deformation regions. As shown earlier in the case of ethanol (Figs. 6 and 7),  $\text{UO}_2^{2+}/\text{MCM-41} + \text{dry air}$  is taken as the reference, so that the bands observed during the in situ FT-IR analysis are due to 2-propanol or the surface complexes/gaseous products formed or depleted during photo-oxidation. Fig. 10 presents spectra of  $\text{UO}_2^{2+}/\text{MCM-41} + 2$ -propanol in the absence of irradiation subtracted from that formed in the presence of irradiation. Thus, the bands shown are due to the surface complexes/gaseous products generated during the photo-oxidation process.

In the absence of irradiation, positive IR bands visible at  $\sim 2975$ ,  $\sim 2928$ ,  $\sim 2887$ ,  $\sim 1465$ ,  $\sim 1386$ , and  $\sim 1340 \text{ cm}^{-1}$  in Fig. 9 correspond to the stretching and deformation vibrations of 2-propanol and/or 2-propoxide (see Table 6 for band assignments) [32–35]. As in the case of ethanol, which exhibited a band at  $\sim 1250 \text{ cm}^{-1}$  due to  $\delta(\text{OH})$ , indicating that it is molecularly adsorbed on  $\text{UO}_2^{2+}/\text{MCM-41}$  in addition to forming an ethoxide with the catalyst, 2-propanol also exhibited a band due to  $\delta(\text{O-H})$  at  $\sim 1251 \text{ cm}^{-1}$  [32,33]. This suggests the presence of some molecularly adsorbed 2-propanol on  $\text{UO}_2^{2+}/\text{MCM-41}$  as  $\text{U-OH} \cdots \text{OH-CH}(\text{CH}_3)_2$  [26], which is also validated by the formation of a broad band at  $\sim 3153 \text{ cm}^{-1}$  due to the hydrogen-bonded O-H stretching frequency  $\nu(\text{OH})$  of 2-propanol [29]. The formation of 2-propoxide with the catalyst as  $\text{U-O-CH}(\text{CH}_3)_2$  can be confirmed by the presence of negative bands at  $\sim 3732$  and  $\sim 3655 \text{ cm}^{-1}$  due to depletion of isolated hydroxyl groups [26] in  $\text{M-OH}$  ( $\text{U-OH/Si-OH}$ ), as shown in Fig. 10. In addition, IR band at  $\sim 1625 \text{ cm}^{-1}$  due to  $\delta(\text{OH})$  of adsorbed water [28–30] shows that water can be formed as a result of 2-propoxide formation on catalyst. The exposure of 2-propanol to  $\text{UO}_2^{2+}/\text{MCM-41}$  in the absence of

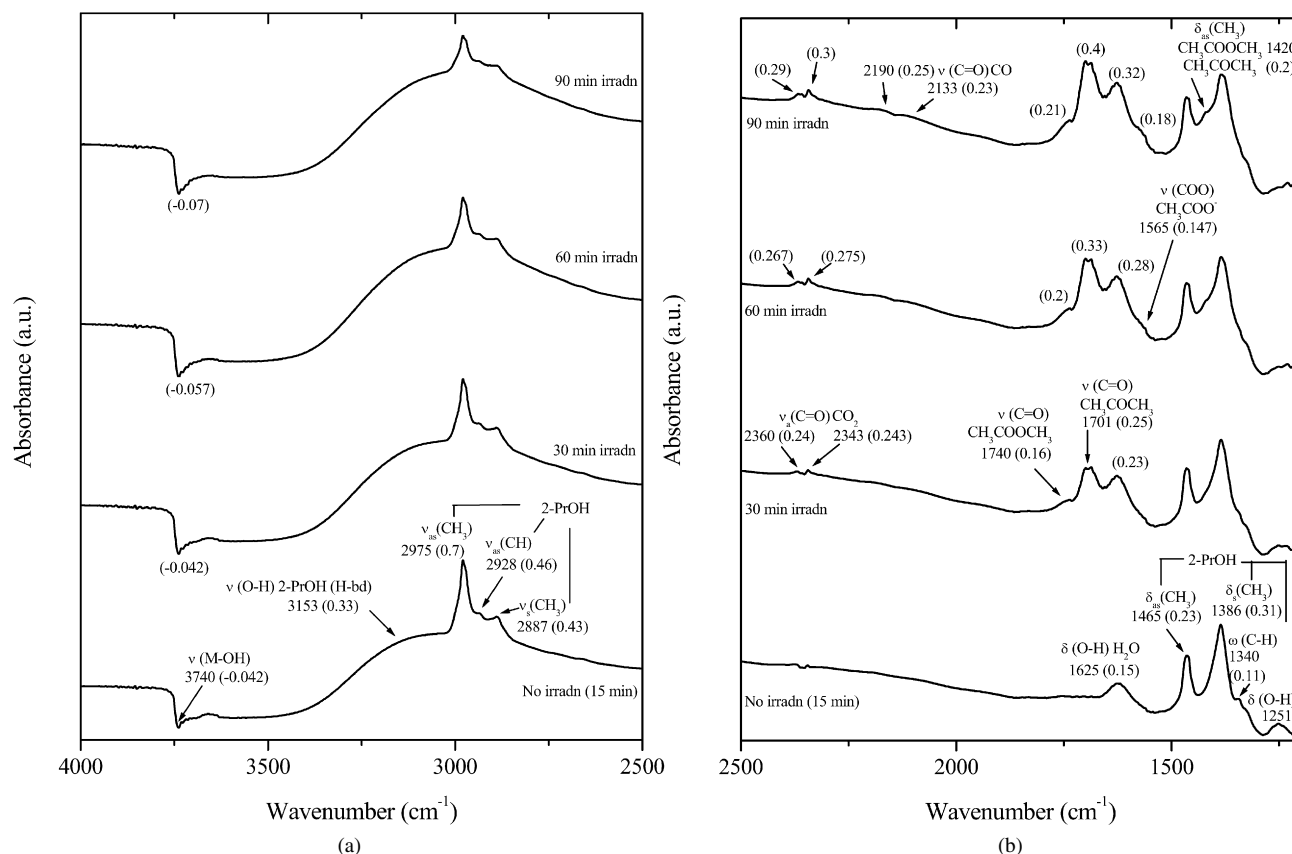


Fig. 9. FT-IR spectra of  $\text{UO}_2^{2+}/\text{MCM-41}$  with 2-propanol prior to and post irradiation in the (a) stretching and (b) deformation regions.

irradiation for 15 min did not result in the formation of any additional bands [16].

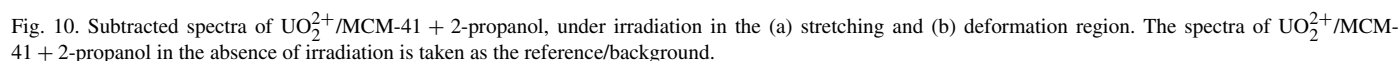
The influence of irradiation of 2-propanol adsorbed on uranyl photocatalyst resulted in the following changes:

- (i) Positive IR bands were formed and were found to grow in intensity with irradiation time, as shown in Figs. 9 and 10. A sharp band at  $\sim 1701 \text{ cm}^{-1}$  was observed, along with a shoulder at  $\sim 1740 \text{ cm}^{-1}$ . Based on the literature, the band at  $\sim 1701 \text{ cm}^{-1}$  was attributed to  $\nu(\text{C=O})$  of acetone [26,29,36], whereas the band at  $\sim 1740 \text{ cm}^{-1}$  was due to  $\nu(\text{C=O})$  of methyl acetate [29–31]. Further, IR bands at  $\sim 1423 \text{ cm}^{-1}$  could be due to  $\delta_{\text{as}}(\text{CH}_3)$  vibrations of methyl acetate [29–31] and acetone [26,29,36], whereas  $\sim 1365 \text{ cm}^{-1}$  was due to  $\delta_{\text{s}}(\text{CH}_3)$  vibration of acetone [26,29,36]. In addition, a band was seen at  $\sim 1565 \text{ cm}^{-1}$ , attributed to the  $\nu_{\text{as}}(\text{COO})$  of acetate species, with the  $\nu_{\text{s}}(\text{COO})$  band at  $\sim 1447 \text{ cm}^{-1}$  [26,37]. The band assignments of the transient species obtained are presented in Table 7.
- (ii) In addition, bands due to formation of carbon dioxide ( $\sim 2360$ ,  $\sim 2343 \text{ cm}^{-1}$ ), carbon monoxide ( $\sim 2190$  and  $\sim 2133 \text{ cm}^{-1}$ ), and water ( $\sim 1627 \text{ cm}^{-1}$ ) increased in intensity with irradiation time [29–31], in line with our photocatalytic results. However, the presence of two  $\nu_{\text{a}}(\text{C=O})$  bands of  $\text{CO}_2$  instead of one band ( $2349 \text{ cm}^{-1}$ ) indicates the presence of both gaseous and bonded  $\text{CO}_2$ . This holds true for CO as well (literature value,  $2127 \text{ cm}^{-1}$ ).

- (iii) Growth of the intermediate species, along with increasing intensity of carbon dioxide and water formed, are functions of irradiation time (Fig. 11). The intensity and time profiles for the growth of acetone differ from those of acetate and methyl acetate, indicating an independent pathway for its formation from 2-propanol/2-propoxide.
- (iv) As was shown for ethanol, an increasing negative band at  $\sim 3732 \text{ cm}^{-1}$  compared with  $\sim 3655 \text{ cm}^{-1}$  suggests the participation of uranyl, not silanol, sites in the photo-oxidation process. The initial adsorption of 2-propanol on the photocatalyst leads to the formation of  $\text{U-OCH}(\text{CH}_3)_2$  and  $\text{Si-OCH}(\text{CH}_3)_2$ , as seen in the negative bands shown in Figs. 9 and 10. However, on irradiation, the photocatalytic process occurs at the uranyl site. The  $\text{Si-OCH}(\text{CH}_3)_2$  groups do not participate in the reaction after irradiation. The increasingly negative absorbance of the  $\text{U-OH}$  bands with irradiation time indicates that the intermediate species acetate, methyl acetate, and acetone bond more strongly at the uranyl site compared with 2-propanol.
- (v) Identical experiments carried out over uranyl-free MCM-41 did not result in the formation of additional bands (not shown here) other than IR bands due to 2-propanol [16].

### 3.5. Reaction mechanism

Based on the above observations, appropriate reaction mechanisms for the photo-oxidation of ethanol and 2-propanol have been proposed, as shown in Schemes 2, 3, 6, and 7. The reaction



Frequency (cm <sup>-1</sup> )				Vibrational mode
2-Propanol	2-Propanol	2-Propoxide		
This work	[32,33]	[34]	[35]	
3153	3305	3305	—	$\nu(\text{OH})$ , H-bonded
2975	2977	2977	2950, 2959	$\nu_{\text{as}}(\text{CH}_3)$
2928	2938	2938	2915, 924	$\nu_{\text{as}}(\text{CH})$
2887	2884	2884	2841, 2857	$\nu_{\text{s}}(\text{CH}_3)$
1465	1472	1472	1464, 1462	$\delta_{\text{as}}(\text{CH}_3)$
1386	1381	1381	1374, 1381	$\delta_{\text{s}}(\text{CH}_3)$
1340	1342	1342	1333, 1328	—CH— wag
1251	1256	1256	—	$\delta(\text{OH})$

The formation of acetic acid over  $\text{UO}_2^{2+}/\text{MCM-41}$  is assumed to occur from molecularly adsorbed ethanol, as observed from the IR data shown in Fig. 6. Scheme 2 describes the formation of acetic acid from ethanol. On the other hand, the formation of acetaldehyde and ethyl acetate over the uranyl

Frequency (cm <sup>-1</sup> )		Vibrational mode	Transient species/ gaseous products
This work	Reported		
1740	1750–1735 [29]	$\nu(\text{C}=\text{O})$	Methyl acetate
1423	1428 [29]	$\delta_{\text{as}}(\text{CH}_3)$	
1701	1702–1689 [36]	$\nu(\text{C}=\text{O})$	Acetone
1423	1422 [36], 1420 [26]	$\delta_{\text{as}}(\text{CH}_3)$	
1365	1368 [26], 1366 [36]	$\delta_{\text{s}}(\text{CH}_3)$	
1565	1583 [26], 1535 [37]	$\nu_{\text{as}}(\text{COO})$	Acetate
1447	1453 [37], 1437 [26]	$\nu_{\text{s}}(\text{COO})$	
2360, 2343	2349 [30,31]	$\nu_{\text{a}}(\text{C}=\text{O})$	Carbon dioxide
2190, 2133	2127 [30,31]	$\nu(\text{C}=\text{O})$	Carbon monoxide
1627	1630 [30,31]	$\delta(\text{O}-\text{H})$	Water

(i) From IR data, hydrogen-bonded ethanol molecules at the uranyl site result in the formation of molecularly adsorbed ethanol (**2a**), which under irradiation forms a carbon-centered radical (**2b**) via hydrogen atom abstraction by  $^*\text{UO}_2^{2+}$ , with the simultaneous reduction of U(VI) to U(V) (see Table 2) [8,9].

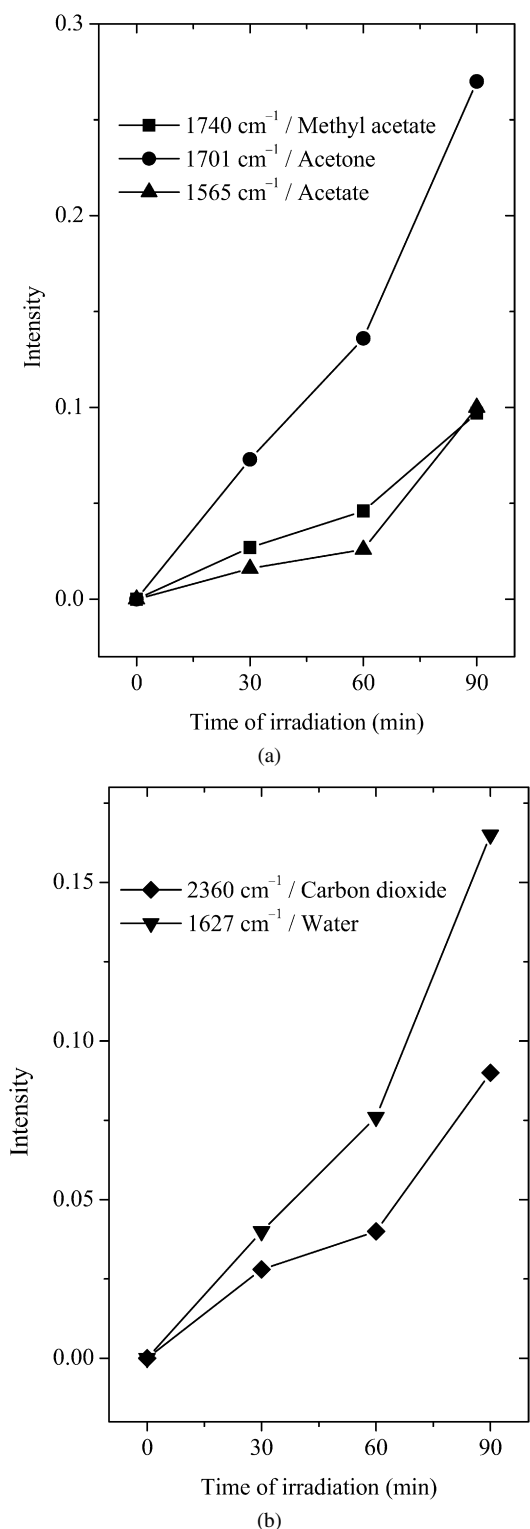


Fig. 11. Plot of intensities of (a) transient species and (b) gaseous products formed during photo-oxidation of 2-propanol over  $\text{UO}_2^{2+}/\text{MCM-41}$ , as a function of irradiation time.

- (ii) In the presence of oxygen, the carbon-centered radical forms ethanol hydroperoxide (**2c**), with the regeneration of  $\text{UO}_2^{2+}$ .
- (iii) Under irradiation, H atom abstraction occurs from ethanol hydroperoxide, forming a carbon-centered radical (**2d**),

with the simultaneous ejection of a hydroxyl group from the hydroperoxide species, forming molecularly bonded acetic acid (**2e**) and water. On further irradiation, acetic acid forms carbon oxides and water, as shown in the IR data.

Scheme 3 describes the independent formation of acetaldehyde and ethyl acetate from ethoxide. The independent pathways for the photo-oxidation of ethanol/ethoxy to acetic acid, ethyl acetate, and acetaldehyde are based on their nearly equal intensities, and similar time profiles, as observed in Fig. 8a.

- (i) From the IR data shown in Figs. 6 and 7, involvement of the  $-\text{OH}$  group attached preferentially to the uranyl site results in the formation of ethoxy species (**3a**) bonded to the uranyl site.
- (ii) Under the influence of irradiation, the bonded ethoxy species forms a carbon-centered radical (**3b**) via H atom abstraction by  $^*\text{UO}_2^{2+}$ , with the simultaneous reduction of U(VI) to U(V) (see Table 2) [8,9].
- (iii) In the presence of oxygen molecules, the carbon-centered radical possibly forms ethoxy hydroperoxide (**3c**), which under irradiation loses one molecule of water to form acetate species (**3d**) bonded to the uranyl site.

#### Pathway I

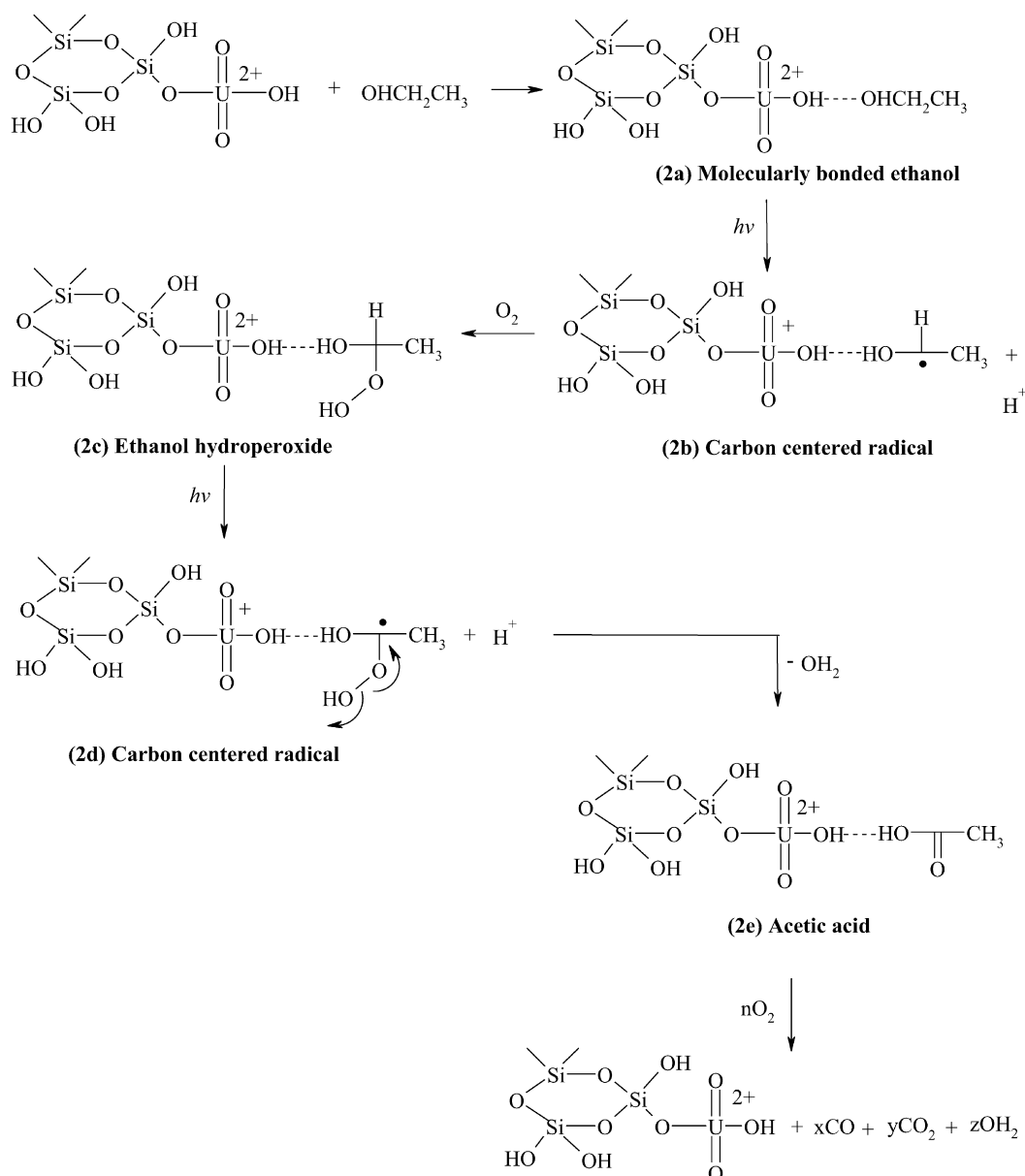
- (iv) Under irradiation and in the presence of ethanol, H atom abstraction by  $^*\text{UO}_2^{2+}$  occurs from ethanol, which attaches itself to the uranyl group, whereas the ethoxy group ( $-\text{OC}_2\text{H}_5$ ) attacks the acetate species, forming ethyl acetate (**3e**).

#### Pathway II

- (v) In a different pathway, under irradiation and in the presence of ethanol, the uranyl-bonded acetate species undergoes hydrogen atom abstraction by  $^*\text{UO}_2^{2+}$ , which attaches itself to the acetate species, forming acetaldehyde (**3f**), hydrogen-bonded to the catalyst. Simultaneously, the ethoxy groups become hydrogen-bonded to the silanol groups.
- (vi) Under the influence of irradiation, hydrogen-bonded ethyl acetate and acetaldehyde undergo further oxidation independently to give carbon oxides and water, with regeneration of the  $\text{UO}_2^{2+}$  catalyst.

#### 3.5.2. 1-Propanol

The reaction pathways for the photo-oxidation of 1-propanol have been extrapolated from those obtained for ethanol on the assumption that the  $1^\circ$  nature of 1-propanol is similar to that of ethanol (Schemes 2 and 3). Based on the mechanism for the oxidation of ethanol, the probable transient species formed over  $\text{UO}_2^{2+}/\text{MCM-41}$  during photo-oxidation of 1-propanol are propionic acid, propanaldehyde, and propyl propionate (Schemes 4 and 5).

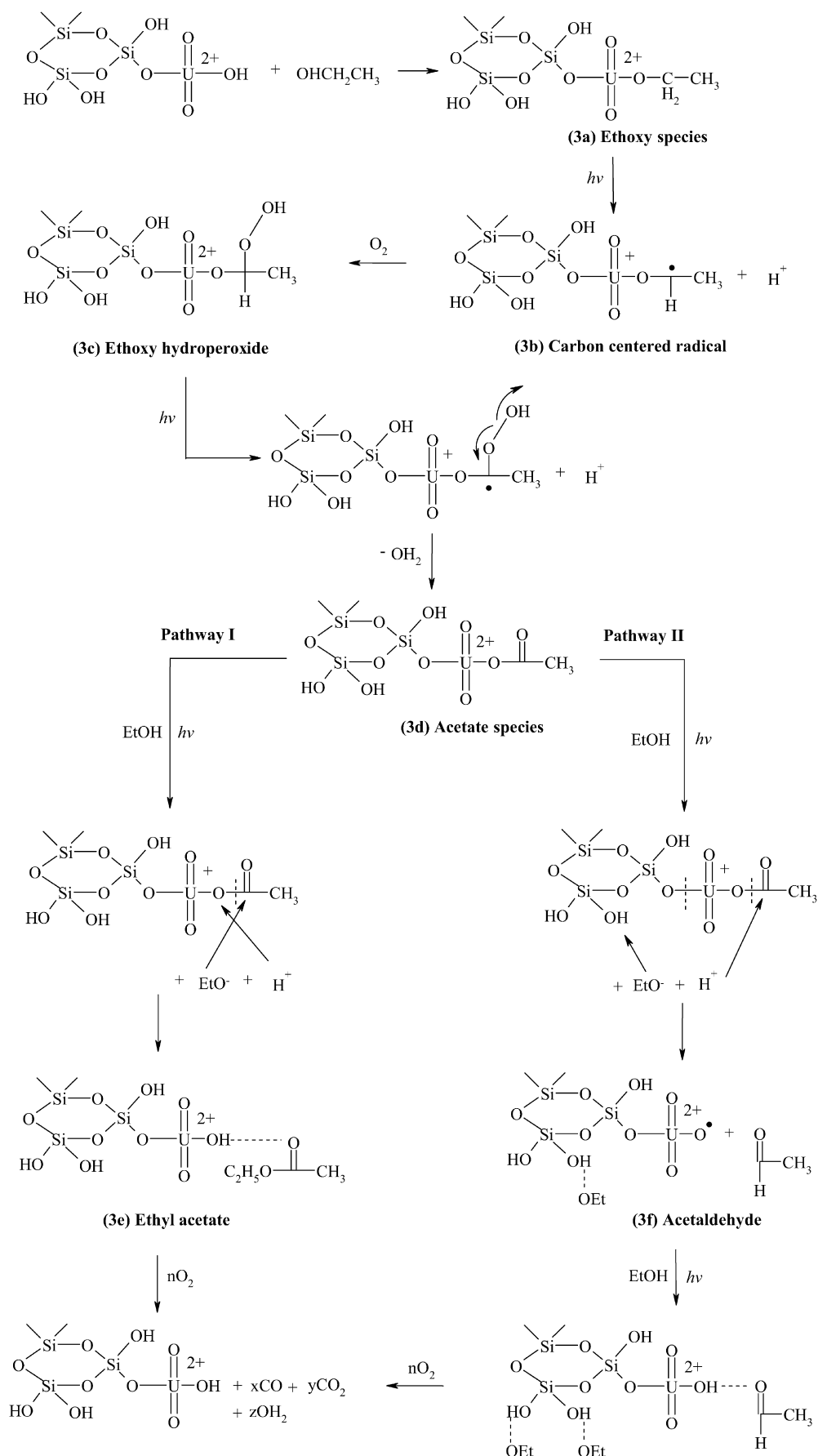
Scheme 2. Photo-oxidation of ethanol over  $UO_2^{2+}/MCM-41$ —Route 1.

### 3.5.3. 2-Propanol

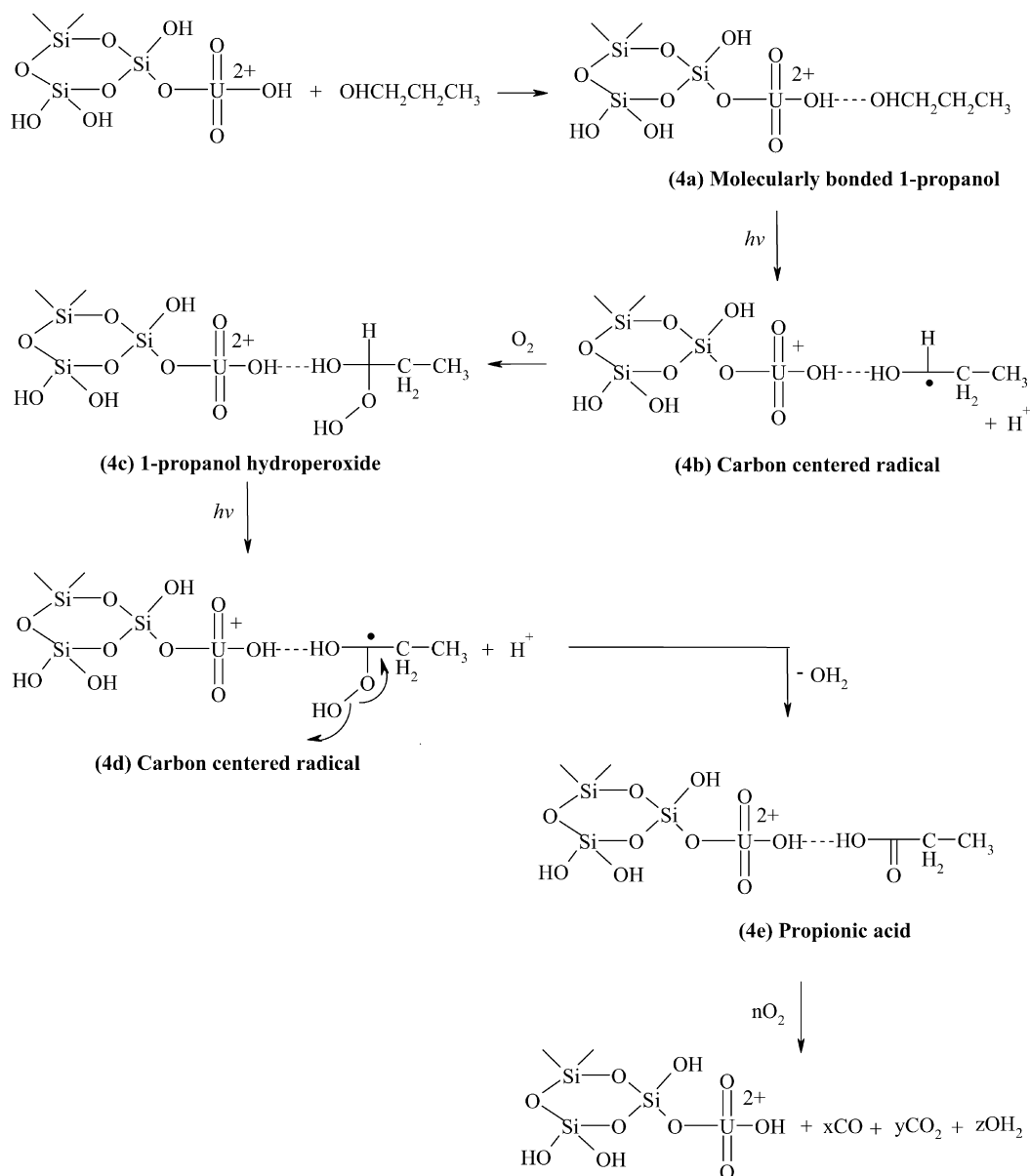
Scheme 6 shows the photo-oxidation mechanism of 2-propanol over  $UO_2^{2+}/MCM-41$ , based on the formation of acetate species (methyl acetate), as shown in Figs. 9 and 10. The gradual formation of acetate species leads us to believe that it is an intermediate species in the formation of methyl acetate (Fig. 11a). On the other hand, the high intensity of acetone species with a different growth pattern than that of acetate and methyl acetate indicates that the oxidation of 2-propanol to acetone takes place via a different pathway, as described in Scheme 7.

- (i) As seen in the case of ethanol, the IR data show involvement of the  $-OH$  group attached preferentially to the uranyl site, resulting in the formation of 2-propoxy species (6a) bonded to the uranyl site.

- (ii) Under irradiation, the bonded 2-propoxy species forms a carbon-centered radical (6b) via H atom abstraction by  $*UO_2^{2+}$ , with the simultaneous reduction of U(VI) to U(V) (see Table 2) [8,9].
- (iii) The carbon-centered radical in the presence of oxygen molecule possibly forms 2-propoxy hydroperoxide (6c). Under irradiation,  $*UO_2^{2+}$  gets quenched by an electron transfer from the methyl radical in 2-propoxy hydroperoxide, forming a carbon-centered radical (6d) and methyl cation, with the simultaneous reduction of U(VI) to U(V). The methyl radical combines with the  $-OH$  group of hydroperoxide, giving methanol and acetate species bonded to the uranyl catalyst (6e).
- (iv) Under irradiation, H atom abstraction by  $*UO_2^{2+}$  occurs from  $CH_3OH$ , which becomes attached to the uranyl

Scheme 3. Photo-oxidation of ethanol over  $\text{UO}_2^{2+}/\text{MCM-41}$ —Route 2.



Scheme 4. Photo-oxidation of 1-propanol over  $\text{UO}_2^{2+}$ /MCM-41—Route 1.

group, whereas  $-\text{OCH}_3$  becomes linked to the acetate species, forming methyl acetate (**6f**).

- (v) Further oxidation of methyl acetate results in the formation of carbon oxides and water, as demonstrated by the IR data shown in Figs. 9 and 10.

#### Scheme 7

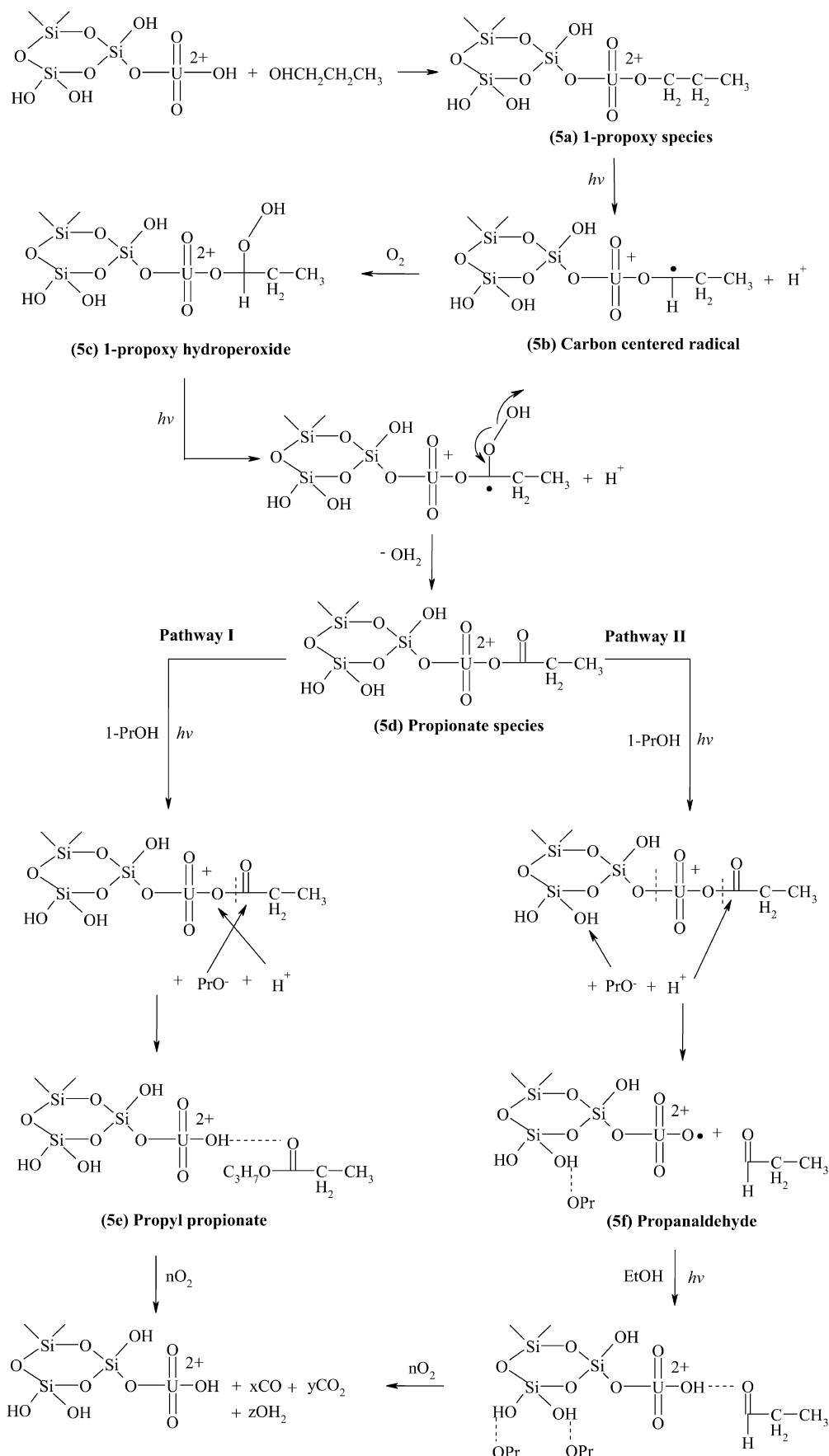
- (i) As shown in Scheme 6, the 2-propoxy species bonded to the uranyl site (**7a**) on irradiation gives rise to the formation of 2-propoxy hydroperoxide in the presence of oxygen (**7b**).
- (ii) Under irradiation and in the presence of 2-propanol, H atom abstraction by  $^*\text{UO}_2^{2+}$  occurs from 2-propanol, which attaches itself to the  $-\text{OH}$  group of the hydroperoxide species, forming water and acetone (**7c**), whereas

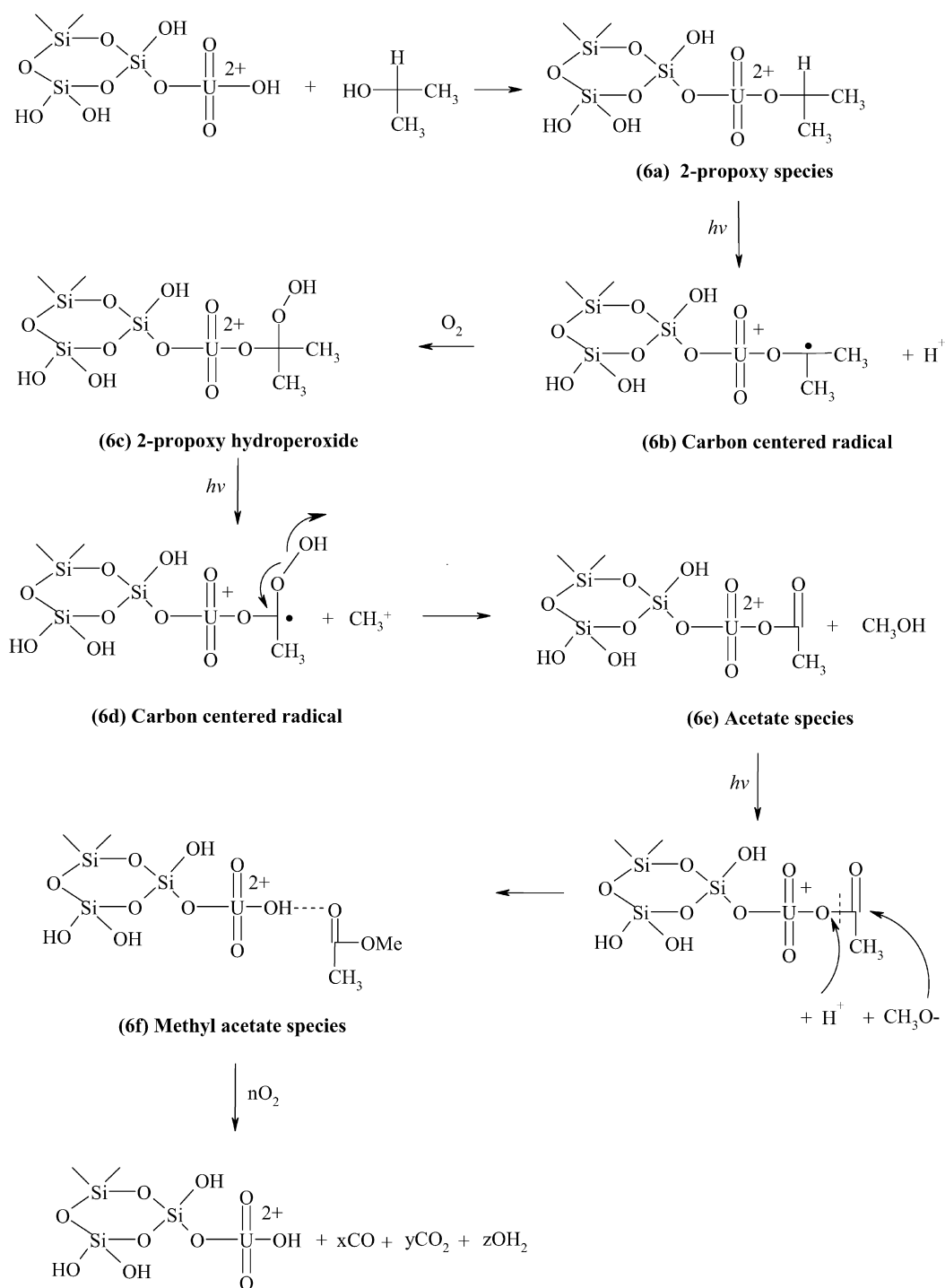
the 2-propoxy group becomes H-bonded to the silanol groups.

- (iii) Subsequently, acetone undergoes further oxidation to give carbon oxides and water, with regeneration of the  $\text{UO}_2^{2+}$  catalyst.

#### 4. Conclusion

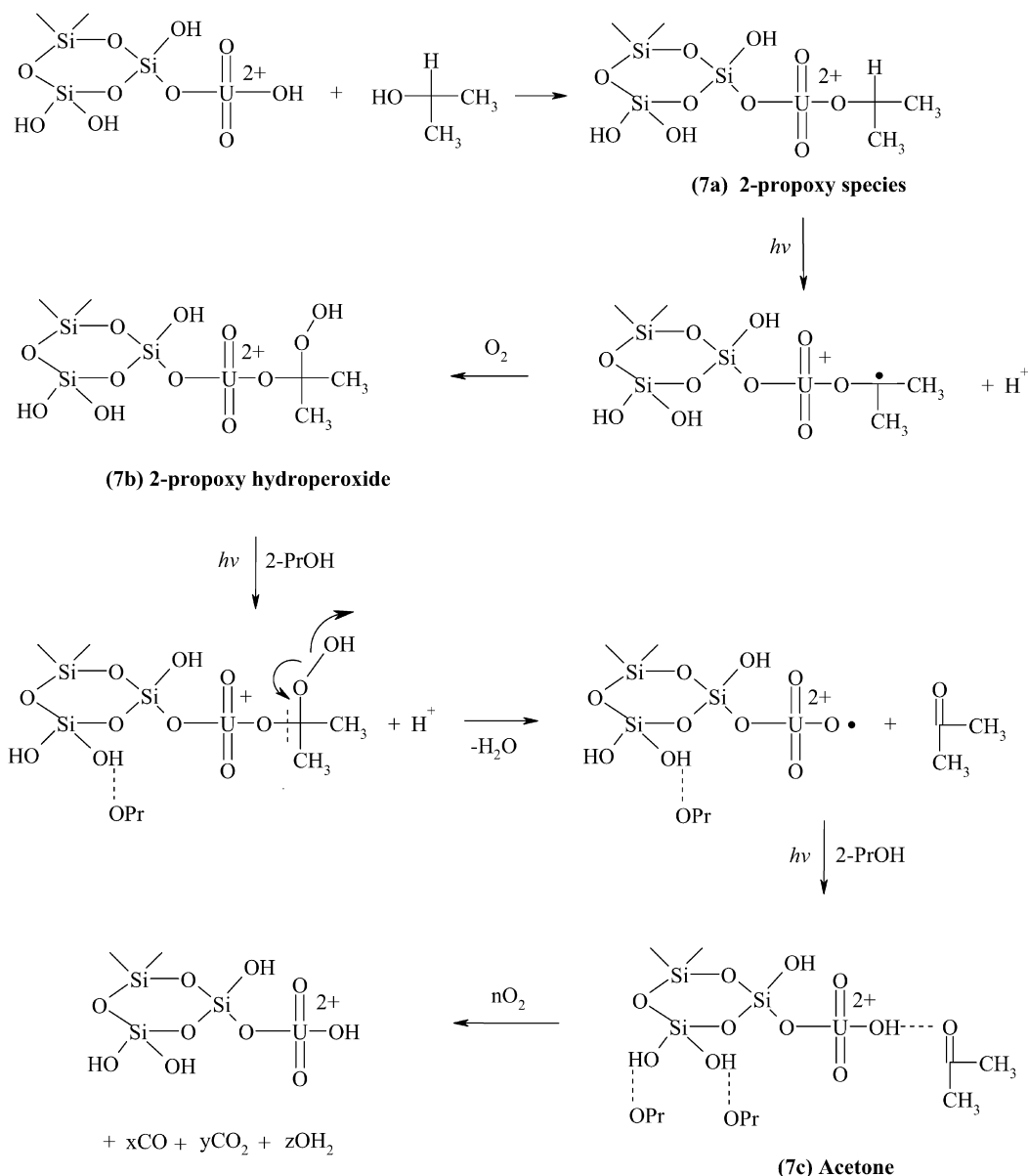
The photo-oxidation of methanol, ethanol, 1-propanol, and 2-propanol was carried out over  $\text{UO}_2^{2+}$ /MCM-41 under ambient conditions, which resulted in their complete degradation. The rate of conversion of alcohols to carbon dioxide followed the order methanol > ethanol > 2-propanol > 1-propanol and was found to depend on the stability of the carbon-centered radicals formed as a result of photo-oxidation. The photo-oxidation of alcohols was found to follow a first-order reaction, with the rate



Scheme 6. Photo-oxidation of 2-propanol over  $\text{UO}_2^{2+}/\text{MCM-41}$ —Route 1.

constants decreasing in the same order as the photocatalytic activity. The transient species formed during the photo-oxidation of these alcohols over  $\text{UO}_2^{2+}/\text{MCM-41}$  were identified by an in situ FTIR technique for the first time. The IR analysis of photo-oxidation of ethanol over  $\text{UO}_2^{2+}/\text{MCM-41}$  gave rise to acetic acid, acetaldehyde, and ethyl acetate, with acetic acid formation occurring over molecularly adsorbed ethanol and acetaldehyde and ethyl acetate formation occurring over ethoxide.

The nearly equal intensities and similar time profiles of acetaldehyde, acetic acid, and ethyl acetate suggest independent pathways for their formation from ethanol/ethoxide groups. On the other hand, the in situ IR study of 2-propanol resulted in the formation of acetate, methyl acetate, and acetone as the transient species. The gradual growth of acetate species with irradiation time demonstrates its conversion to form methyl acetate. Further, the high intensity and different growth pattern of acetone is indicative of an independent

Scheme 7. Photo-oxidation of 2-propanol over  $\text{UO}_2^{2+}/\text{MCM-41}$ —Route 2.

pathway for its formation. Apart from the transient species, gaseous products such as carbon dioxide, carbon monoxide, and water were also detected in the IR analysis, conforming to our photoactivity results. Based on the formation of these intermediates, along with their intensities and time profiles, appropriate reaction mechanisms to establish the role of  $^*\text{UO}_2^{2+}$  in the photo-oxidation of alcohols have been proposed.

## Acknowledgments

The authors thank Professor K.D. Deodhar for his valuable suggestions on the mechanistic data. This work was performed under BRNS contract No. 99/37/BRNS/1049.

## References

- [1] N. Irving Sax, R.J. Lewis, *Hawley's Condensed Chemical Dictionary*, Van Nostrand Reinhold, New York, 1987.
- [2] B. Ramachandran, H.L. Greene, S. Chatterjee, *Appl. Catal. B* 8 (1996) 157.
- [3] A.A. Meharg, D. Osborn, *Nature* 375 (1995) 353.
- [4] M.L.H. Green, R.M. Lago, S.C.J. Tang, *J. Chem. Soc. Chem. Commun.* 365 (1995).
- [5] M.A. Fox, M.T. Dulay, *Chem. Rev.* 93 (1993) 341.
- [6] R. Hoffmann, S.T. Martin, W. Choi, D.W. Bahnemann, *Chem. Rev.* 95 (1995) 69.
- [7] L. Spanhel, H. Weller, A. Henglein, *J. Am. Chem. Soc.* 109 (1987) 6632.
- [8] H.D. Burrows, T.J. Kemp, *Chem. Soc. Rev.* 3 (1974) 139.
- [9] E. Rabinowitch, R.L. Belford, *Spectroscopy and Photochemistry of Uranyl Compounds*, Pergamon, London, 1964.
- [10] W.-D. Wang, A. Bakac, J.H. Espenson, *Inorg. Chem.* 34 (1995) 6034.

- [11] T.M. Bergfeldt, W.L. Waltz, X. Xu, P. Sedlak, U. Dreyer, H. Mockel, J. Lilie, J.W. Stephenson, *Can. J. Chem.* 81 (2003) 219.
- [12] M. Sarakha, M. Bolte, H.D. Burrows, *J. Phys. Chem. B* 104 (2000) 3142.
- [13] S.L. Suib, A. Kostapapus, D.J. Psaras, *J. Am. Chem. Soc.* 106 (1984) 1614.
- [14] S.L. Suib, K.A. Carrado, *Inorg. Chem.* 24 (1965) 863.
- [15] S. Dai, D.H. Metcalf, G.D. Del Cul, L.M. Toth, *Inorg. Chem.* 35 (1996) 7786.
- [16] K. Vidya, V.S. Kamble, P. Selvam, N.M. Gupta, *Appl. Catal. B* 54 (2004) 145.
- [17] V. Krishna, V.S. Kamble, P. Selvam, N.M. Gupta, *Catal. Lett.* 98 (2004) 113.
- [18] K. Vidya, V.S. Kamble, N.M. Gupta, P. Selvam, *Stud. Surf. Sci. Catal.* 156 (2005) 787.
- [19] K. Vidya, N.M. Gupta, P. Selvam, *Mater. Res. Bull.* 39 (2004) 2035.
- [20] G.L. Wesley, G.S. Forbes, *J. Am. Chem. Soc.* 52 (1930) 3139.
- [21] K. Bhattacharyya, S. Varma, K. Kishore, N.M. Gupta, *Res. Chem. Int.* 32 (2005) 17.
- [22] D. Kumar, S. Bera, A.K. Tripathi, G.K. Dey, N.M. Gupta, *Micropor. Mesopor. Mater.* 66 (2003) 157.
- [23] A.G. Robiette, J.L. Duncan, *Annu. Rev. Phys. Chem.* 34 (1983) 255.
- [24] D. Kumar, G.K. Dey, N.M. Gupta, *Phys. Chem. Chem. Phys.* 5 (2003) 5477.
- [25] D.R. Lide, *CRC Handbook of Chemistry and Physics*, CRC Press, London, 1999.
- [26] J.M. Coronado, S. Katoaka, I. Tejedor-Tejedor, M.A. Anderson, *J. Catal.* 219 (2003) 219.
- [27] J. Araña, J.M. Doña-Rodríguez, I. Garriga, C. Cabo, O. González-Díaz, J.A. Herrera-Melián, J. Pérez-Peña, *Appl. Catal. B* 53 (2004) 221.
- [28] W.C. Wu, C.C. Chuang, J.L. Lin, *J. Phys. Chem. B* 104 (2000) 8719.
- [29] R.M. Silverstein, *Spectrometric Identification of Organic Compounds*, Wiley, Canada, 1963.
- [30] J. Chalmers, P. Griffiths, *Handbook of Vibrational Spectroscopy*, Wiley, New York, 2002.
- [31] K. Nakamoto, *Infrared and Raman Spectra of Inorganic and Coordination Compounds*, Wiley, New York, 1978.
- [32] L.J. Shorthouse, A.J. Roberts, R. Raval, *Surf. Sci.* 480 (2001) 37.
- [33] J.B. Benzinger, R.J. Madix, *J. Catal.* 65 (1980) 36.
- [34] P. Uvdal, B.C. Wiegand, J.G. Serafin, C.M. Friend, *Phys. Rev. B* 51 (12) (1995) 7884.
- [35] M.K. Weldon, C.M. Friend, *Chem. Rev.* 96 (1996) 1391.
- [36] M. El-Maazawi, A.N. Finken, A.B. Nair, V.H. Grassian, *J. Catal.* 191 (2000) 138.
- [37] L.F. Liao, W.C. Wu, C.Y. Chen, J.L. Lin, *J. Phys. Chem. B* 105 (2001) 7678.